

INTEGRAL constraints on the Galactic hard X-ray background from the Milky Way anticenter^{*}

R. Krivonos^{1,2}, S. Tsygankov^{1,2,3,4}, M. Revnivtsev², S. Sazonov², E. Churazov^{1,2}, R. Sunyaev^{1,2}

¹ Max-Planck-Institut für Astrophysik, Karl-Schwarzschild-Str. 1, D-85740 Garching bei München, Germany

² Space Research Institute, Russian Academy of Sciences, Profsoyuznaya 84/32, 117997 Moscow, Russia

³ Finnish Centre for Astronomy with ESO (FINCA), University of Turku, Väisäläntie 20, FI-21500 Piikkiö, Finland

⁴ Astronomy Division, Department of Physics, FI-90014 University of Oulu, Finland

the date of receipt and acceptance should be inserted later

Abstract. We present results of a study of the Galactic ridge X-ray emission (GRXE) in hard X-rays with the IBIS telescope on board INTEGRAL in the region near the Galactic Anticenter (GA) at $l = 155^\circ$. We assumed a conservative 2σ upper limit on the flux from the GA in the 25 – 60 keV energy band of 1.25×10^{-10} erg s⁻¹ cm⁻² (12.8 mCrab) per IBIS field of view, or 6.6×10^{-12} erg s⁻¹ cm⁻² (0.7 mCrab) per degree longitude in the $135^\circ < l < 175^\circ$ region. This upper limit exceeds the expected GRXE intensity in the GA direction by an order of magnitude, given the near-infrared (NIR) surface brightness of the Milky Way in this region and the standard hard X-ray-to-NIR intensity ratio for the GRXE, assuming stellar origin. Based on the CGRO/EGRET surface brightness of the Galaxy above 100 MeV as a tracer of the cosmic-ray (CR) induced gamma-ray background, the expected GRXE flux in GA exceeds the measured 2σ upper limit by a factor of 4. Therefore, the non-detection of hard X-ray emission from the GA does not contradict the stellar nature of the GRXE, but is inconsistent with CR origin.

Key words. galaxy: structure – X-rays: diffuse background

1. Introduction

The stellar origin of the Galactic hard X-ray background, better known as the Galactic ridge X-ray emission (GRXE), has recently been strongly supported by morphological/spectral studies with the RXTE and INTEGRAL observatories (Revnivtsev et al. 2006; Krivonos et al. 2007a; Türler et al. 2010), spectral studies with Suzaku (Ebisawa et al. 2008; Yamauchi et al. 2008) and direct X-ray source counts with Chandra (Revnivtsev et al. 2009, 2011). The GRXE does not arise from the interaction of cosmic rays with the interstellar medium, as was believed before, but is associated with the (predominantly old) stellar population of the Galaxy, namely with hard X-ray emission from accreting white dwarfs and coronally active stars. It was demonstrated (Revnivtsev et al. 2006; Krivonos et al. 2007a) that the GRXE intensity closely follows near-infrared (NIR) sur-

face brightness over the Milky Way, which is a known tracer of stellar mass.

Galactic diffuse emission in a region far away from the Galactic Center (GC) was studied by Worrall et al. (1982) with the A2 experiment on board the HEAO1 satellite. The observed 2 – 10 keV emission was consistent with an radial exponential disk with a half-thickness of ~ 240 pc. It was pointed out that unresolved emission likely comes from discrete point sources and does not have a diffuse origin. In the hard X-ray domain GRXE was studied by Skibo et al. (1997) using OSSE observations at longitude $l = 95^\circ$. The observed emission between 50 and 600 keV was suspected to contain a significant contribution from bright discrete sources because of the wide collimated field of view ($\sim 11^\circ.4 \times 3^\circ.8$), but a major part of the detected flux was interpreted as interstellar emission from non-thermal electrons (see also e.g. Valinia et al. 2000; Valinia & Tatischeff 2001). Today, thanks to the unique possibilities of INTEGRAL gamma-ray telescopes, we can directly study the Galactic diffuse background in any parts of the Galaxy without dealing with significant source contamination.

^{*} Based on observations with INTEGRAL, an ESA project with instruments and science data centre funded by ESA member states (especially the PI countries: Denmark, France, Germany, Italy, Switzerland, Spain), Czech Republic and Poland, and with the participation of Russia and the USA

Given the distribution of $4.9\mu\text{m}$ NIR intensity over the Galaxy as measured by the COBE/DIRBE experiment, the GRXE is not expected to be detectable in the Galactic Anticenter (GA) because of the low NIR surface brightness in this region. Nevertheless, an explicit demonstration that the GRXE is not observed from a Galactic region of low stellar density, such as the GA, would substantiate the stellar paradigm of the GRXE even more. Placing tight constraints on the hard X-ray flux from the GA region is also important for calibrating future studies of the GRXE in the central parts of the Galaxy.

2. Observations

We used data from the ISGRI detector, the first layer of the IBIS coded-mask telescope (Ubertini et al. 2003), on board the INTEGRAL gamma-ray observatory (Winkler et al. 2003). ISGRI operates at energies above ~ 20 keV, with the sensitivity rapidly decreasing above 100 keV. IBIS has a relatively wide field of view ($\sim 28^\circ \times 28^\circ$ at zero response), which allows one to measure weak diffuse emission fluxes by using the telescope as a collimated instrument.

To study the GRXE in the GA region, we used special INTEGRAL observations, part of a series of so-called Galactic latitude scans (*GLS*). This program is based on consecutive observations made along the Galactic latitude in the range $\pm 30^\circ$ with a step of 2° . This strategy allows one to make independent snapshot measurements of the instrumental background at mid latitudes, where the GRXE is expected to be negligible, along with an actual GRXE observation near the Galactic plane. It is crucial that the instrumental background, which is usually high in hard X-ray observations, does not exhibit strong variability during an individual *GLS* lasting ~ 8 hours.

There are two positions in the GA region observed with *GLS*s: ongoing observations at $l = 215^\circ$ (PI: Tsygankov) and a completed program at $l = 155^\circ$ with a total exposure of 1 Ms (PI: Krivonos). In the present study we only used the completed *GLS* observations at $l = 155^\circ$ performed in August–September 2010, see Table 1 for details. After screening the whole data set following the procedure described in Krivonos et al. (2007a), hereafter K07, we were left with 525 out of 569 short (~ 2 ks) individual INTEGRAL observations, called *scientific windows* (*ScWs*), for the subsequent scientific analysis. To model background variations we used public data of high-latitude observations (Table 1).

3. Analysis

We mainly followed the approach described in K07. Our study of the GRXE is based on the capability of the IBIS telescope to separate the contributions of point sources from the background count rate.

The ISGRI detector shadowgram that was accumulated during individual INTEGRAL observation in a given energy range was cleaned from source fluxes using the

Table 1. INTEGRAL observations used for the GRXE study.

Latitude scan at $l = 155^\circ$, 2010		
Observation field	Orbits	<i>ScWs</i>
...	960,961	2–94,11–97
...	962,963	12–112,1–97
...	964,965	13–110,2–67
...	966	23–56
569 <i>ScWs</i> , total nominal exposure: 1 Ms.		
Background model calibration, 2008–2009		
Observation field	Orbits	
North Ecliptic Pole	686–689, 759–761, 824–829	
XMM-LSS	695, 696, 701	
Virgo Cluster	747–754, 758, 819–820	
Coma Cluster	821–823	
M82 X-1	869–872	
3C273, 3C279 and M87	878–880	
Total nominal exposure: 6 Ms.		
Crab calibration, 2010		
Observation field	Orbits	
Crab Nebula	902, 903, 966–968, 970	
Total nominal exposure: 890 ks.		

known pattern of the IBIS mask. The remaining shadowgram contains the following components: (i) variable instrumental background, (ii) the isotropic cosmic X-ray background (CXB), and (iii) the GRXE. Throughout the analysis we assumed the CXB flux as a constant part of the instrumental background. The possible influence of the CXB variance on the GRXE measurement is considered in Appendix B. Because the GRXE is extended over the sky, it cannot be directly resolved with the IBIS mask. The only way to estimate the GRXE flux is to determine the difference between the observed collimated detector count rate that is cleaned from sources and the assumed instrumental background. To this end, we define a background model in Appendix A that predicts the background count rate during a given GRXE observation. The background model is adjusted very precisely using mid-latitude snapshots of the background performed shortly before and after a given GRXE observation, which is the main concept of the *GLS*.

3.1. Detector shadowgram

Because IBIS is a coded aperture imaging telescope, the sky is projected onto the detector plane through the transparent and opaque elements of the mask mounted above the detector plane. We produced the ISGRI detector shadowgram for every *ScW* as described in K07. We used the 25 – 60 keV working energy band because of the known evolution of the low-energy threshold of the ISGRI detector and because the GRXE is expected to be weak above ~ 50 keV owing to the high-energy cut-off in the GRXE spectrum (Krivonos et al. 2007a; Revnivtsev et al. 2006).

3.2. Sky map

The sky reconstruction is based on deconvolution of the detector shadowgram with a known mask pattern. We implemented the IBIS/ISGRI sky reconstruction method described in our previous publications (Revnivtsev et al. 2004; Krivonos et al. 2005, 2007a,b). For the basic idea we refer the reader to the papers by Fenimore & Cannon (1981) and Skinner et al. (1987). Every sky image was additionally cleaned from systematic noise as described in Krivonos et al. (2010a). The resulting sky image mosaic is shown in Fig. 1.

The survey area as a function of flux for sources with $S/N > 5$ is shown in Fig. 2. The minimum detectable flux in the central part of the field is 2.4×10^{-11} erg s^{-1} cm^{-2} (or 2.5 mCrab). The survey area reaches its geometric limit of 3650 deg² for $f > 4.9 \times 10^{-9}$ erg s^{-1} cm^{-2} (500 mCrab), 50% of this area has a sensitivity better than 8.1×10^{-11} erg s^{-1} cm^{-2} (8.3 mCrab).

We performed a search for sources as excesses in the sky mosaic (Fig. 1) convolved with a Gaussian representing the effective instrumental PSF. The detection threshold was estimated assuming Gaussian noise of the pixel values as follows. The total area of the sky image (Fig. 1) is 3650 squared degrees, and taking the IBIS telescope angular resolution of 12' into account, we gathered $\sim 9.12 \times 10^4$ independent pixels. With this consideration, we set the source detection threshold to 5σ , allowing at most one false detection for pure Gaussian noise.

The signal-to-noise ratio distribution of pixels shown in Fig. 3 has the expected Gaussian shape. However, one notices some systematic excess at the negative side. Nevertheless, the source detection threshold of 5σ , estimated above, separates the noise and source dominated pixel domains.

The list of point sources is presented in Table 2. We attribute two marginally detected, previously unknown sources to the systematic noise. IGR J08135+5655 is not detected in the sky mosaic of the slightly broader energy band 20 – 60 keV, and the region around IGR J01532+2612 is affected by systematic noise at the edge of the sky mosaic.

The list of sources in Table 2, except for two IGR's mentioned above, was used in the iterative source removal (IROS) procedure that we applied to every ISGRI detector shadowgram (e.g. Krivonos et al. 2010a). This procedure introduces additional uncertainty to the background model (Appendix C), but allows one to trace source variability. For example, the known Be/X-ray binary RX J0440.9+4431 (LS V +44 17) was in a strong outburst during the observations (Krivonos et al. 2010c; Tsygankov et al. 2011). Fig. 4 shows 25 – 60 keV detector light curve, cleaned from the source contribution, and ready for further analysis.

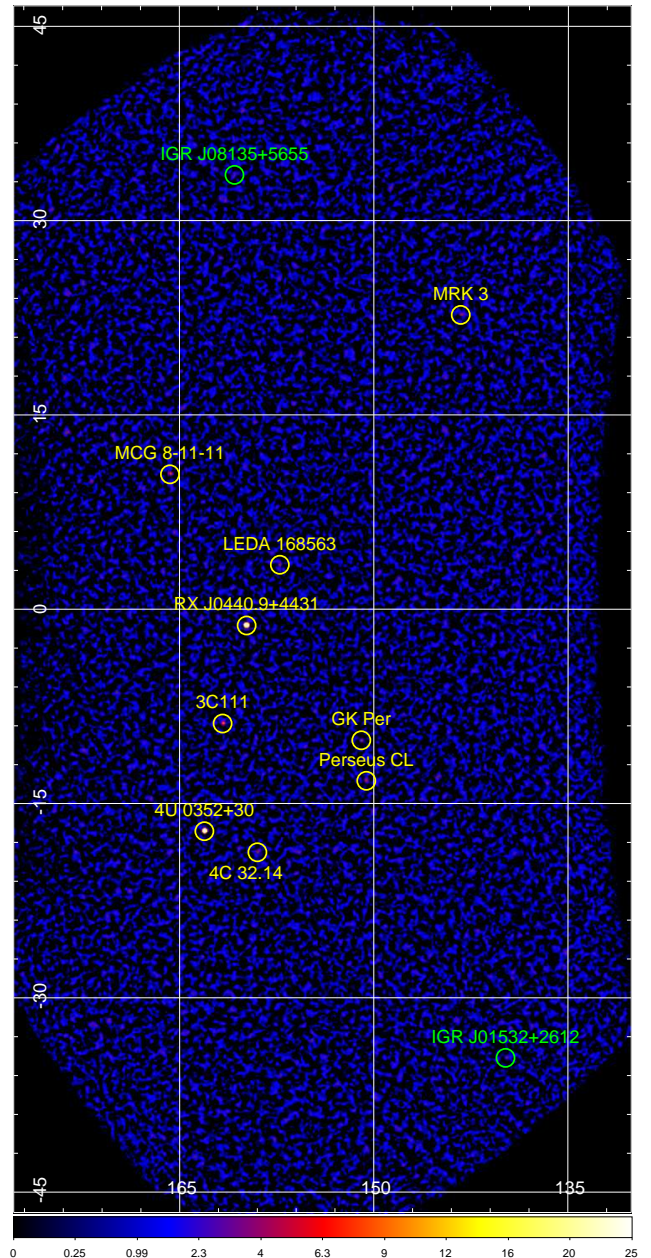


Fig. 1. IBIS/ISGRI sky image of the 1 Ms observation of the GA region at $l = 155^\circ$ produced in the 25 – 60 keV energy range. The color table of the image represents pixel values in the range 0-25 calculated as the square root of the significance. The cataloged and newly detected sources are labeled in yellow and green, respectively.

4. Results

Using the background model (Appendix A) we obtained for each ScW the predicted detector count rate, as shown in Fig. 5. The detailed view of the observed and predicted detector light curves and their residuals during a spacecraft orbit 964 is shown in Fig. 6. We denoted regions of background measurement ($|b| \geq 20^\circ$) in blue, and actual

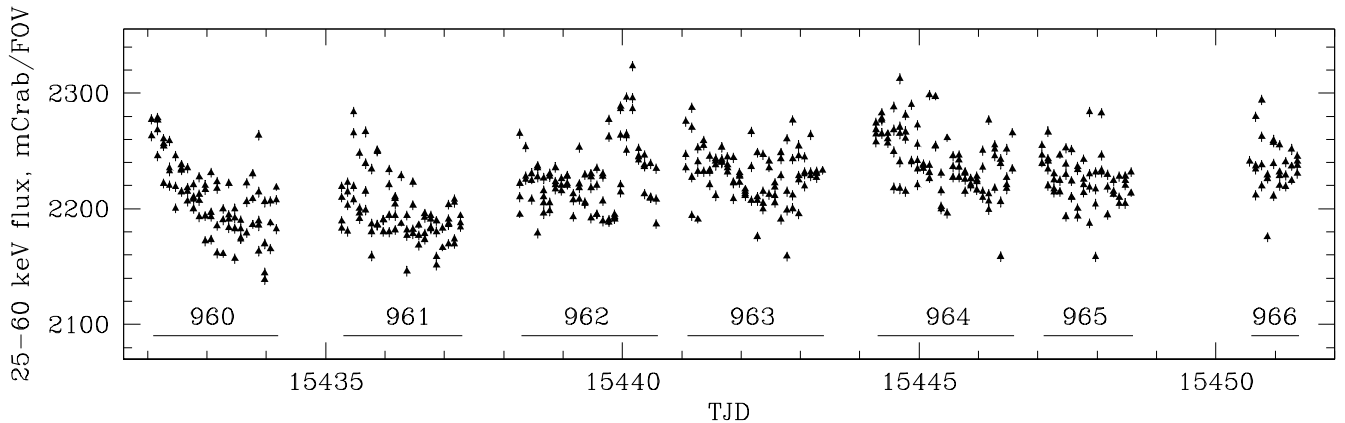


Fig. 4. Detector count rate of the individual *ScWs* after subtracting flux contribution from point sources during the *GLS* program at $l = 155^\circ$. The data points contain pure statistical errors. The labeled horizontal intervals denote different spacecraft orbits.

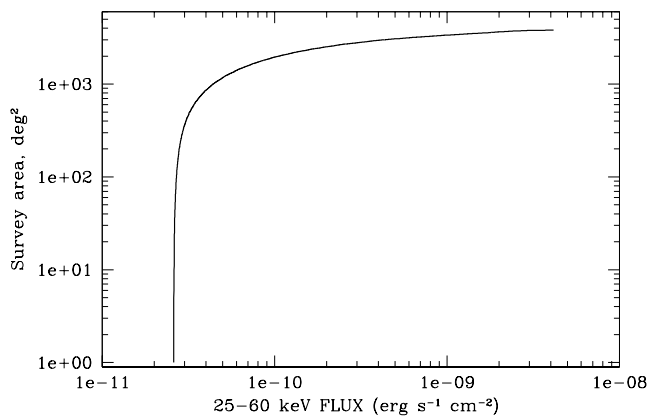


Fig. 2. Covered area of the survey as a function of flux for sources with $S/N > 5$

GRXE observations ($|b| < 20^\circ$) in red. Fig. 6 shows that the background behavior in an individual orbit can be captured only with fast scanning observations such as *GLSs*. The background model, with low intrinsic scatter, exactly follows the observed detector rate, and the scatter of residuals (lower panel of Fig. 6) is comparable to the statistical uncertainty of the IROS procedure (Appendix C).

Using the entire *GLS* data set at $l = 155^\circ$, we averaged residuals over Galactic latitude, as shown in Fig. 7 by red points. The latitude profile does not show any significant excess in the Galactic plane region at $b = 0^\circ$. As expected, the GRXE associated with the old stellar population is not detected in the GA. The 1σ upper limit on the GRXE flux in the $|b| < 5^\circ$ latitude range, which roughly corresponds to the IBIS fully coded FOV, is ~ 2.8 mCrab, or ~ 6.4 mCrab taking systematic uncertainties into account. We later refer to a 2σ upper limit of ~ 12.8 mCrab. One can convert the achieved upper limit to more convenient units using the effective solid angle of the IBIS telescope ~ 286 deg 2 and taking into account that the GRXE is much less extended in the Galactic latitude than the average cross-section of IBIS FOV. For instance, the 2σ upper

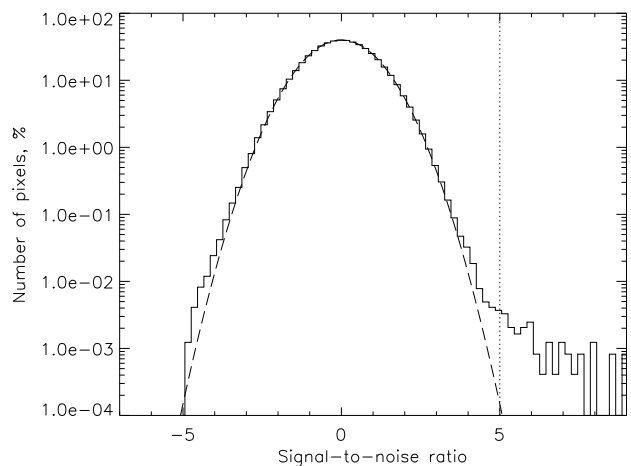


Fig. 3. Signal-to-noise ratio distribution of pixels in the 1 Ms *GLS* observation at $l = 155^\circ$. The dashed line represents the normal distribution with unit variance and zero mean. The accepted threshold of source detection (5σ) is shown by the dotted line. The plot is truncated at $\sigma = 9$ for convenience.

limit on the GRXE flux at $l = 155^\circ$ per unit Galactic longitude is 0.7 mCrab deg $^{-1}$.

One can test the GRXE non-detection in the GA for consistency with stellar and truly diffuse GRXE origins. To this end, we compared the observed drop of the hard X-ray flux from the GC to the GA region (per IBIS FOV) with the corresponding change of the intensity of a given tracer. We used the COBE/DIRBE $4.9\mu\text{m}$ data¹ as a tracer of stellar mass, and the EGRET gamma-ray background map above 100 MeV as a tracer of the cosmic-ray induced gamma-ray background. The EGRET background intensity drops from the GC to the GA by a factor of ~ 3 . Therefore, using the conservative estimate of the GRXE flux in the GC from K07 of 150 ± 15 mCrab,

¹ COBE/DIRBE $4.9\mu\text{m}$ intensity map was corrected for the interstellar reddening and mean background level measured in high-latitude regions, as described in K07.

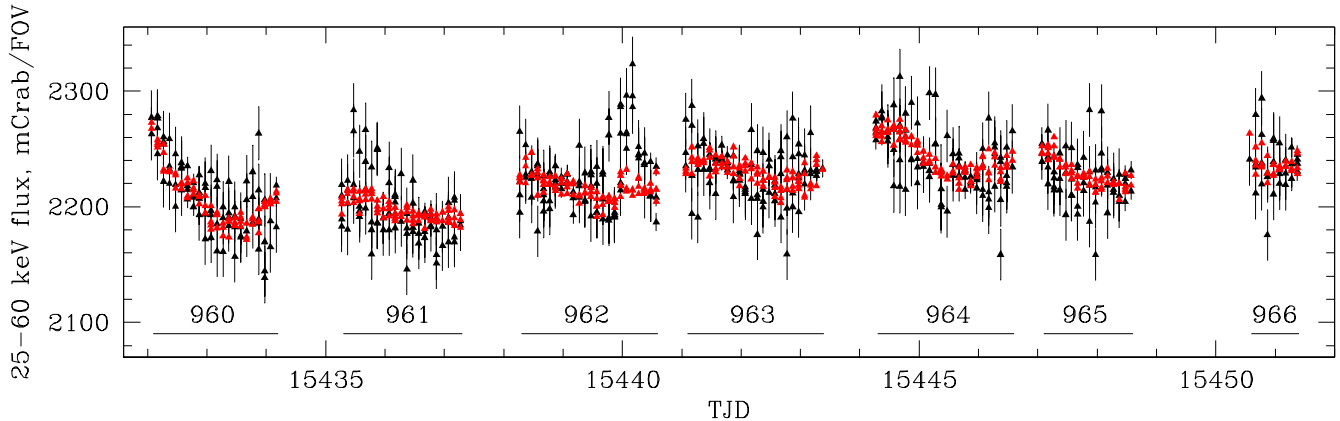


Fig. 5. Detector count rate (black) of the individual *ScWs* as shown in Fig. 4. The systematic uncertainty of the source removal procedure (Appendix C) was added to the statistical errors of each point. The red points represent the count rate predicted by the background model.

Table 2. The list of sources significantly ($\geq 5\sigma$) detected on the sky mosaic (Fig. 1). The newly detected sources are highlighted in bold. The 68% confidence interval for estimated sky coordinates depends on source significance: $2.1'$, $1.5'$, and $< 0.8'$ for $5 - 6, 10$, and $> 20\sigma$, respectively (Krivonos et al. 2007b)

Name	lon. deg.	lat. deg.	$F_{25-60 \text{ keV}}$ mCrab
4U 0352+30 ^a	163.08	-17.14	39.42 ± 0.69
RX J0440.9+4431 ^a	159.82	-1.26	26.12 ± 0.53
3C111 ^b	161.68	-8.83	5.32 ± 0.60
MCG 8-11-11 ^b	165.74	10.41	7.27 ± 0.86
4C 32.14 ^c	158.99	-18.77	3.15 ± 0.56
LEDA 168563 ^b	157.26	3.43	2.76 ± 0.49
MRK 3 ^b	143.29	22.72	7.23 ± 1.33
Perseus CL ^d	150.58	-13.25	3.06 ± 0.58
IGR J01532+2612	139.82	-34.64	20.31 ± 3.91
IGR J08135+5655	160.75	33.53	7.09 ± 1.38
GK Per ^e	150.96	-10.12	2.82 ± 0.56

^a HMXB, ^b AGN, ^c QSO, ^d Cluster of Galaxies, ^e CV

we expect the corresponding flux from the GA to be ~ 50 mCrab. This is definitely not observed according to Fig. 7. In contrast, there is a factor of 270 drop in the NIR $4.9\mu\text{m}$ intensity from $2.7 \times 10^{-5} \text{ erg s}^{-1} \text{ cm}^{-2}$ to $10^{-7} \text{ erg s}^{-1} \text{ cm}^{-2}$. This implies a GRXE flux from the GA of 0.4 mCrab at 25 – 60 keV, which is consistent with the derived upper limit of 12.8 mCrab. This is illustrated in Fig. 8, where the COBE/DIRBE and EGRET longitude profiles are renormalized to the hard X-ray flux observed from the GC. We conclude that the non-detection of the GRXE from the GA is consistent with the stellar mass distribution of the Galaxy traced by NIR maps, rather than with the cosmic-ray induced gamma-ray background seen by EGRET.

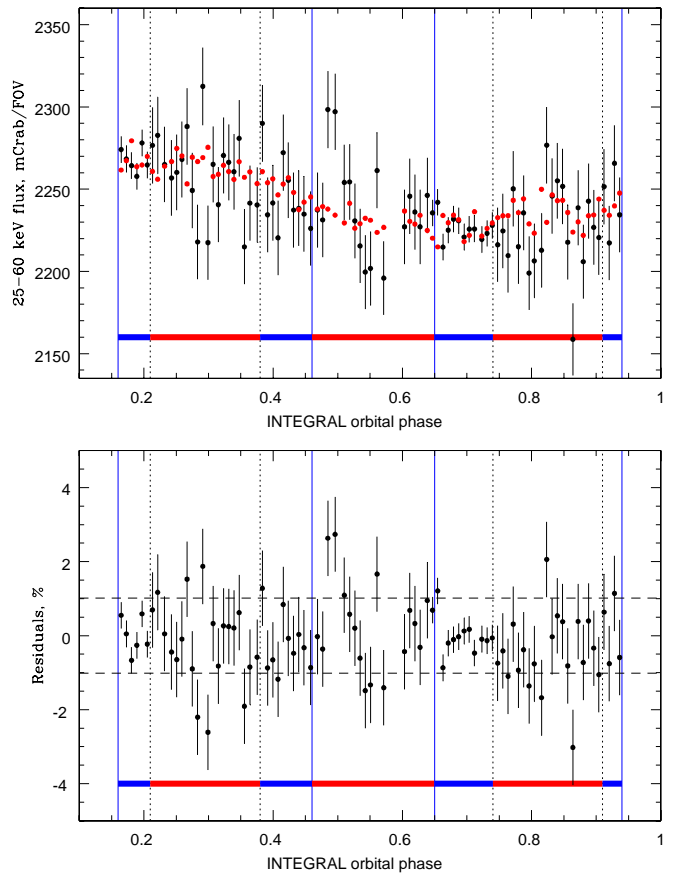


Fig. 6. *Upper panel:* Detailed view of detector count rate (black) during orbit 964 from Fig. 5. The blue and red areas denote observations made at $|b| \geq 20^\circ$ and $|b| < 20^\circ$, respectively. *Bottom panel:* Residuals after subtracting the model-predicted count rate from the observed count rate. The black dashed lines represent a 1σ deviation (1.02%) from zero.

5. Conclusions

1) Using the 1 Ms observations of the GA at $l = 155^\circ$ with the INTEGRAL observatory, performed in the spe-

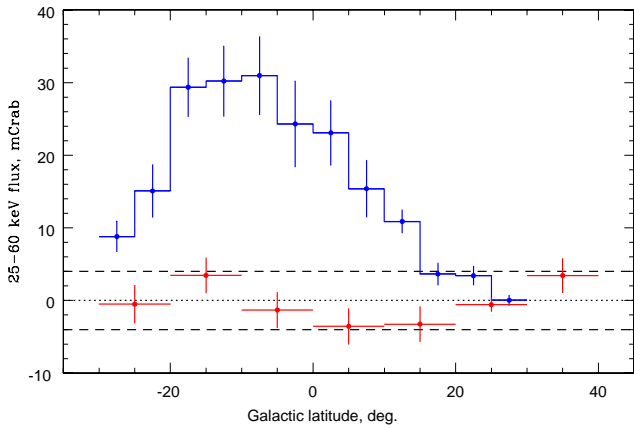


Fig. 7. Source flux contribution (blue) and ISGRI detector background count rate residuals (red) averaged over the Galactic latitude. Error bars of the blue histogram represent rms-deviations of the summed point source fluxes from average in bin.

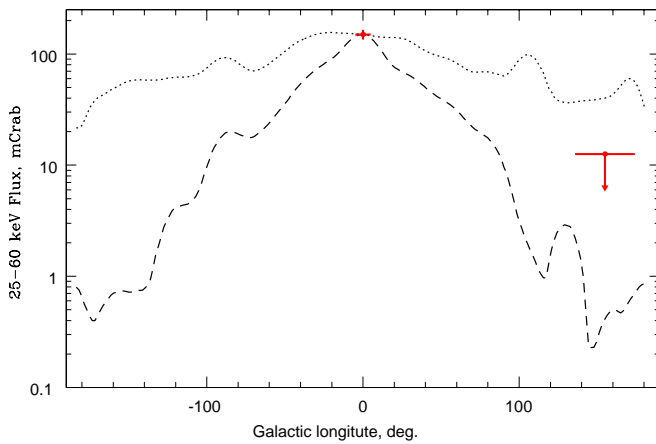


Fig. 8. Galactic longitude profiles of the COBE/DIRBE $4.9\mu\text{m}$ intensity (dashed line) and EGRET background above 100 MeV (dotted line), both normalized to the GRXE flux of 150 mCrab (red point) in the GC. The 2σ upper limit corresponds to the GRXE measurement at $l = 155^\circ$ in the present study.

cial *GLS* mode, we did not detect the GRXE in the 25 – 60 keV energy band and set a conservative 2σ upper limit of $1.25 \times 10^{-10} \text{ erg s}^{-1} \text{ cm}^{-2}$ (12.8 mCrab) per IBIS FOV or $6.6 \times 10^{-12} \text{ erg s}^{-1} \text{ cm}^{-2} \text{ deg}^{-1}$ (0.7 mCrab deg^{-1}) per unit Galactic longitude.

2) The obtained upper limit is consistent with the considerable drop in the NIR (4.9μ) intensity observed by COBE/DIRBE and disagrees with the much smaller decrease in the gamma-ray (above 100 MeV) background measured by EGRET. Therefore, the non-detection of the GRXE in the GA is consistent with the stellar mass distribution in the Galaxy, which does not contradict the stellar nature of GRXE, but is inconsistent with its CR origin.

3) The developed background model potentially allows one to reach the statistically limited accuracy. However, the final uncertainty of the approach is associated with the source removal procedure, the systematic uncertainty of the method itself, and the CXB variance. Nevertheless, the implemented method along with the special *GLS* mode of observation is an optimal approach of modeling the ISGRI background and can be efficiently used for studying the Galactic hard X-ray background.

Acknowledgements. This research was made possible thanks to the unique capabilities of the INTEGRAL observatory. The data used were obtained from the European and Russian INTEGRAL Science Data Centers. The work was supported by the President of the Russian Federation (through the program of support of leading scientific schools, project NSH-5069.2010.2, and grant MD-1832.2011.2), by the Presidium of the Russian Academy of Sciences/RAS (the program “Origin, Structure, and Evolution of Objects of the Universe”), by the Division of Physical Sciences of the RAS (the program “Extended objects in the Universe”, OFN-16), by the Russian Basic Research Foundation (grant 10-02-00492-A), State contract 14.740.11.0611, and the Academy of Finland grant 127512.

References

- Churazov, E., et al. 2007, *A&A*, 467, 529
 Ebisawa, K., et al. 2008, *PASJ*, 60, 223
 Fabian, A. C., & Barcons, X. 1992, *ARA&A*, 30, 429
 Fenimore, E. E., Cannon T. M., 1981 *Applied Optics*, 20, 1858.
 Skinner, G. K., Ponman, T. J., Hammersley, A. P., & Eyles, C. J. 1987, *Astroph.Sp.Sci.*, 136, 337
 Gruber, D. E., Matteson, J. L., Peterson, L. E., & Jung, G. V. 1999, *ApJ*, 520, 124
 Hajdas W., Bühler P., Eggel C., Favre P., Mchedlishvili A., Zehnder A., 2003, *A&A*, 411, L43
 Krivonos, R., Vikhlinin, A., Churazov, E., Lutovinov, A., Molkov, S., & Sunyaev, R. 2005, *ApJ*, 625, 89
 Krivonos, R., Revnivtsev, M., Churazov, E., Sazonov, S., Grebenev, S., & Sunyaev, R. 2007, *A&A*, 463, 957
 Krivonos, R., Revnivtsev, M., Lutovinov, A., Sazonov, S., Churazov, E., & Sunyaev, R. 2007, *A&A*, 475, 775
 Krivonos, R., Revnivtsev, M., Tsygankov, S., Sazonov, S., Vikhlinin, A., Pavlinsky, M., Churazov, E., & Sunyaev, R. 2010a, *A&A*, 519, A107
 Krivonos, R., Tsygankov, S., Revnivtsev, M., Grebenev, S., Churazov, E., & Sunyaev, R. 2010b, *A&A*, 523, A61
 Krivonos, R., Tsygankov, S., Lutovinov, A., Turler, M., & Bozzo, E. 2010c, *The Astronomer’s Telegram*, 2828, 1
 Revnivtsev, M., Sunyaev, R., Varshalovich, D., et al. 2004, *Astronomy Letters*, 30, 382
 Revnivtsev, M., Sazonov, S., Gilfanov, M., Churazov, E., & Sunyaev, R. 2006, *A&A*, 452, 169
 Revnivtsev, M., Molkov, S., & Sazonov, S. 2008, *A&A*, 483, 425
 Revnivtsev, M., Sazonov, S., Churazov, E., Forman, W., Vikhlinin, A., & Sunyaev, R. 2009, *Nature*, 458, 1142

- Revnivtsev, M., Sazonov, S., Forman, W., Churazov, E., & Sunyaev, R. 2011, MNRAS, 414, 495
- Skibo, J. G., et al. 1997, ApJ, 483, L95
- Tsygankov, S., Krivonos, R., Lutovinov, A., 2011, MNRAS, submitted
- Türler, M., Chernyakova, M., Courvoisier, T. J.-L., Lubiński, P., Neronov, A., Produit, N., & Walter, R. 2010, A&A, 512, A49
- Ubertini P., et al., 2003, A&A, 411, L131
- Valinia, A., Kinzer, R. L., & Marshall, F. E. 2000, ApJ, 534, 277
- Valinia, A., & Tatischeff, V. 2001, Exploring the Gamma-Ray Universe, 459, 153
- Winkler C., et al., 2003, A&A, 411, L1
- Worrall, D. M., Marshall, F. E., Boldt, E. A., & Swank, J. H. 1982, ApJ, 255, 111
- Yamauchi, S., Ebisawa, K., Tanaka, Y., Koyama, K., Matsumoto, H., Yamasaki, N. Y., Takahashi, H., & Ezoe, Y. 2008, arXiv:0810.0317

Appendix A: Background model

The background model used in K07 was slightly changed in this study. Since the *GLS* observations were performed over a relatively short time period, we removed the long-term time part from the equation. Instead of using the gain parameter to trace orbital modulations of the background rate, we used the spacecraft orbital phase P in a quadratic polynomial form. Hereafter, we consider only the detector count rates after removal of the contribution of point sources. The model of the detector background 25 – 60 keV count rate, D_{bgd} , is made of a linear combination of the 600 – 1000 keV detector count rate, H , and phase

$$D_{bgd} = const + aH + b_1P + b_2P^2. \quad (\text{A.1})$$

The coefficient a was calculated using observations pointed away from the Galactic plane ($|b| > 20^\circ$) where the GRXE is not expected to be observed (see Table 1). The constant term and b coefficients were determined individually for each spacecraft orbit from the observations at $|b| > 20^\circ$, thus adjusting the model to the current background level. In fact, the constant term in Eq. A.1 contains contribution from CXB and unknown intrinsic detector background. The last is also variable, which is traced by variability of this constant with time. In the current observations, its absolute value varies in the range of 800 – 900 mCrab from orbit to orbit, while permanent CXB contribution is expected to be at level of 550 mCrab (Appendix B). Finding the difference between the observed and predicted by Eq. A.1 detector count rate should yield the GRXE excess in the Galactic plane.

The detector count rate was converted to the convenient units of Crab flux, with $1 \text{ mCrab} = 7.25 \times 10^{-6} \text{ cts/s}$ in the 25 – 60 keV band per IBIS FOV. The conversion coefficient was determined from observations of the Crab Nebula in 2010 (Table 1). A flux of 1 mCrab in

the 25 – 60 keV energy band corresponds to $9.7 \times 10^{-12} \text{ erg s}^{-1} \text{ cm}^{-2}$ for a source with a Crab-like spectrum, $10.0 \times E_{\text{keV}}^{-2.1} \text{ phot cm}^{-2} \text{ s}^{-1} \text{ keV}^{-1}$.

Appendix B: CXB cosmic variance

The CXB emission coming from the population of unresolved extragalactic sources (active galactic nuclei, AGNs) is subject to Poissonian variations in the number of sources, intrinsic source variability, and nearby large-scale structure (see e.g. Fabian & Barcons 1992). Here, we estimate the systematic limitations to the measured GRXE flux caused by CXB variations.

Using the extragalactic $\log N$ – $\log S$ relation from Krivonos et al. (2010b) and following Revnivtsev et al. (2008), we estimated the relative uncertainty of the CXB flux in the 25 – 60 keV band as

$$\left(\frac{\delta I_{\text{CXB}}}{I_{\text{CXB}}} \right)_\Omega \sim 5.5 \times 10^{-2} S_{\text{max},11}^{1/4} \Omega_{\text{deg}}^{-1/2}, \quad (\text{B.1})$$

where $S_{\text{max},11}$ is the maximum flux of undetected sources in units of $10^{-11} \text{ erg s}^{-1} \text{ cm}^{-2}$, and $\Omega_{\text{deg}} \approx 286$ is the effective solid angle of the IBIS telescope. We adopted the CXB intensity to be equal to $1.89 \times 10^{-11} \text{ erg s}^{-1} \text{ cm}^{-2} \text{ deg}^{-2}$, based on the CXB spectrum model of Gruber et al. (1999) and the $\sim 10\%$ higher normalization measured by INTEGRAL (Churazov et al. 2007). Using the limiting flux of the survey Eq. B.1 yields a CXB variance at the level of $\sim 0.4\%$. The absolute value is 2.3 mCrab assuming a $\sim 550 \text{ mCrab}$ CXB flux per IBIS FOV. In the current work, we consider the CXB variance for an area of three IBIS FOVs, which approximately corresponds to the effective area of the GA survey.

Appendix C: Uncertainty in GRXE measurements

The uncertainty of the background model, i.e. the accuracy of the ISGRI background rate prediction, is subject to statistical and systematic errors. The former can be easily estimated from the total number of counts ($\sim 3 \times 10^5$) in the 25 – 60 keV energy band per typical *ScW* ($\sim 2 \text{ ks}$).

The additional statistical effect is related to the IROS procedure, when the count rate attributed to a given source is removed from the detector using the known aperture function of the mask. To a first approximation, the total number of counts, S , associated with a given source is determined as the difference between the number of counts, D_1 , in the detector pixels illuminated by the source through the mask and the number of counts, D_0 , in the detector pixels blocked by the mask: $S = D_1 - D_0$. The total flux on the detector is $D = D_0 + D_1$. Thus, subtracting the contribution of the source yields the residual detector flux $D' = D - S = 2D_0$. For a weak source in the center of the field of view, $D_0 \approx D_1 \approx 1/2 \times D$ and therefore the relative statistical uncertainty of measuring the detector count rate $\frac{D'}{\sqrt{2D_0}} = \sqrt{2} \frac{D}{\sqrt{D}}$ increases by a factor of $\sqrt{2}$. In practice, a more complicated model of a point source (see

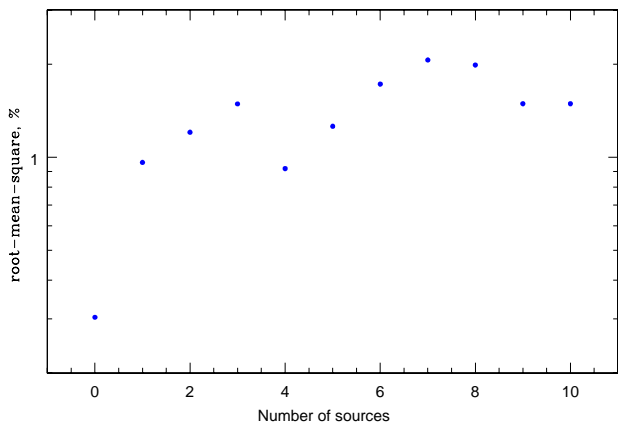


Fig. C.1. Relative root-mean-squared value of the detector rate as a function of number of sources in the FOV.

K07), implemented in the source subtraction algorithm, causes an even larger increase of statistical uncertainties.

To estimate the IROS induced uncertainty as a function of number of sources in the FOV, we studied a set of 22 consecutive observations without cataloged and detected sources (orbit 973, *ScWs* 58 – 80). The relative standard deviation of detector count rate, as a function of the number of simulated sources, N_{src} , is shown in Fig C.1. The first point at $N_{src} = 0$, $RMS = 0.3\%$, reflects the relative statistical scatter of the data. As seen from Fig C.1, the scatter rapidly increases with inclusion of sources in the FOV. A typical scatter of $\sim 1.0\%$ on the *ScW* time scale is observed in real data, as demonstrated in Sect. 4.

To estimate the systematic uncertainty of the method, we defined coefficients of the background model in Eq. A.1 using the high-latitude observations (see Table 1) in the South Galactic hemisphere (700 ks) and applied it to the North (5.3 Ms). The non-existent GRXE flux was averaged over a given INTEGRAL orbit divided into the three equal intervals having three parts: one in the middle and two adjacent, see Fig. C.2 for reference. The middle part of each interval (in red) was supposed to have GRXE flux, and the neighboring parts (in blue) were used to correct the constant term (Eq.A.1). This set-up mimics the *GLS* pattern of observations.

The standard deviation of residuals from zero represents the systematic uncertainty of our background model, which is found to be ~ 4.0 mCrab. The 25 – 60 keV detector count rate increased from ~ 2.2 to ~ 2.5 Crab over the considered time period, hence the relative accuracy of the model is $\sim 0.17\%$ of the observed background rate.

We summarize all the discussed uncertainties related to the GRXE measurements in the 25 – 60 keV energy band. The values below are presented with respect to the background rate, which is assumed to be 2.5 Crab.

Statistical uncertainties:

- 0.18% (4.5 mCrab) – count statistics, *expected* for 3×10^5 counts per typical *ScW* (~ 2 ks),

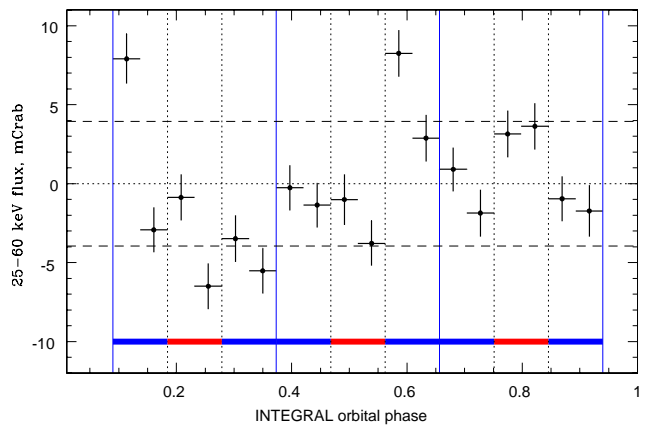


Fig. C.2. Residuals after subtracting the model-predicted count rate from the observed count rate for the 5.3Ms high-latitude observations averaged over spacecraft orbital phase. The black dashed lines represent a 1σ deviation (4.0 mCrab) of the averaged values from zero. Blue and red regions denote different phase intervals used for background model calibration and actual measurements, respectively.

- 0.30% (7.5 mCrab) – count statistics, *observed* in a typical *ScW* without any sources in the FOV. Since this value differs from the expected, it cannot be fully statistical. Some unexplored systematics or background variability can contribute to the scatter of the observed detector count rate.
- 1.00% (25 mCrab) – observed in a typical *ScW* with several sources in the FOV, related to the IROS procedure.

These uncertainties constitute the error of measurement and, naturally, decrease with increasing exposure. For example, the largest error of 25 mCrab decreases to 1 mCrab for a total exposure of 1 Ms. *Systematic uncertainties:*

- 0.16% (4.0 mCrab) – root-mean-squared residuals after background model subtraction from the observed count rate (Fig. C.2),
- 0.09% (2.3 mCrab) – CXB variance per IBIS FOV,
- 0.16% (4.0 mCrab) – CXB variance per GA survey area.

The systematics quadratically add to the error of the measurement. The total systematic error owing to the background model and CXB variance (per GA survey area) is 5.7 mCrab.